

# Chemical Science

Accepted Manuscript



This article can be cited before page numbers have been issued, to do this please use: Y. Zhang, G. Ye, S. Soni, X. Qiu, T. L. Krijger, H. Jonkman, M. Carlotti, E. Sauter, M. Zharnikov and R. Chiechi, *Chem. Sci.*, 2018, DOI: 10.1039/C8SC00165K.



This is an Accepted Manuscript, which has been through the Royal Society of Chemistry peer review process and has been accepted for publication.

Accepted Manuscripts are published online shortly after acceptance, before technical editing, formatting and proof reading. Using this free service, authors can make their results available to the community, in citable form, before we publish the edited article. We will replace this Accepted Manuscript with the edited and formatted Advance Article as soon as it is available.

You can find more information about Accepted Manuscripts in the [author guidelines](#).

Please note that technical editing may introduce minor changes to the text and/or graphics, which may alter content. The journal's standard [Terms & Conditions](#) and the ethical guidelines, outlined in our [author and reviewer resource centre](#), still apply. In no event shall the Royal Society of Chemistry be held responsible for any errors or omissions in this Accepted Manuscript or any consequences arising from the use of any information it contains.

# Controlling Destructive Quantum Interference in Tunneling Junctions Comprising Self-assembled Monolayers via Bond Topology and Functional Groups

Yanxi Zhang,<sup>†,‡,¶</sup> Gang Ye,<sup>†,‡,¶</sup> Saurabh Soni,<sup>†,‡</sup> Xinkai Qiu,<sup>†,‡</sup> Theodorus L. Krijger,<sup>†,‡</sup> Harry T. Jonkman,<sup>‡</sup> Marco Carloti,<sup>†,‡</sup> Eric Sauter,<sup>§</sup> Michael Zharnikov,<sup>§</sup> and Ryan C. Chiechi<sup>\*,†,‡</sup>

<sup>†</sup>*Stratingh Institute for Chemistry, University of Groningen, Nijenborgh 4, 9747 AG Groningen, The Netherlands*

<sup>‡</sup>*Zernike Institute for Advanced Materials, Nijenborgh 4, 9747 AG Groningen, The Netherlands*

<sup>¶</sup>*These authors contributed equally to this work.*

<sup>§</sup>*Applied Physical Chemistry, Heidelberg University, Im Neuenheimer Feld 253, Heidelberg 69120, Germany*

E-mail: r.c.chiechi@rug.nl



## ABSTRACT

Quantum interference effects (QI) are of interest in nano-scale devices based on molecular tunneling junctions because they can affect conductance exponentially through minor structural changes. However, their utilization requires the prediction and deterministic control over the position and magnitude of QI features, which remains a significant challenge. In this context, we designed and synthesized three benzodithiophenes based molecular wires; one linearly-conjugated, one cross-conjugated and one cross-conjugated quinone. Using eutectic Ga-In (**EGaIn**) and CP-AFM, we compared them to a well-known anthraquinone in molecular junctions comprising self-assembled monolayers. By combining density functional theory and transition voltage spectroscopy, we show that the presence of an interference feature and its position can be controlled independently by manipulating bond topology and electronegativity. This is the first study to separate these two parameters experimentally, demonstrating that the conductance of a tunneling junction depends on the position and depth of a QI feature, both of which can be controlled synthetically.



## INTRODUCTION

Molecular electronics is concerned with the transport of charge through molecules spanning two electrodes,<sup>[1]</sup> the fabrication of which is a challenging area of nanotechnology.<sup>[2–4]</sup> In such junctions,  $\pi$ -conjugated molecules influence transport more than a simple, rectangular tunneling barrier; when a tunneling electron traverses the region of space occupied by orbitals localized on these molecules, its wave function can undergo constructive or destructive interference, enhancing or suppressing conductance. When the presence of different pathways in molecular system affects conductance, it is typically described as quantum interference (QI),<sup>[5]</sup> which was originally adapted from the Aharonov-Bohm effect<sup>[6]</sup> to substituted benzenes.<sup>[7,8]</sup> The concept “quantum interference effect transistor” was also proposed using meta-benzene structures for device application.<sup>[9]</sup> Solomon et al. further refined the concept in the context of Molecular Electronics where it is now well established that destructive QI leads to lower conductance in tunneling junctions.<sup>[10–15]</sup> We previously demonstrated QI in SAM-based junctions using a series of compounds based on an anthracene core; **AC**, which is linearly-conjugated; **AQ**, which is cross-conjugated via a quinone moiety; and **AH**, in which the conjugation is interrupted by saturated methylene bridges (Figure S1).<sup>[16]</sup> Subsequent studies verified these findings in a variety of experimental platforms and a consensus emerged that, provided the destructive QI feature (anti-resonances in transmission) is sufficiently close to the Fermi level,  $E_F$ , cross-conjugation leads to QI.<sup>[17–24]</sup> However, experimental studies on conjugation patterns other than **AC/AQ** are currently limited to ring substitutions such as *meta*-substituted phenyl rings,<sup>[25–32]</sup> or varied connectivities in azulene,<sup>[33–35]</sup> which differ fundamentally<sup>[5,11,36–38]</sup> from cross-conjugated bond topologies<sup>[23,39,40]</sup> because they change tunneling pathways, molecular-lengths and bond topology simultaneously (Table S1). Isolating these variables is however important because the only primary observable is conductance, which varies exponentially with molecular length. More recent work has focused on “gating” QI effects by controlling the alignment of  $\pi$ -systems through-space<sup>[37,41,42]</sup> and affecting the orbital symmetry of aromatic rings with heteratoms.<sup>[43–45]</sup> These studies exclusively study



the effects of the presence and absence of QI features; to date—and despite recent efforts<sup>[46]</sup>—the specific effects of bond topology and electronegativity on the depth and position of QI features have not been isolated experimentally.

To address this issue, we designed and synthesized the series of benzodithiophene derivatives (**BDT-*n***); benzo[1,2-b:4,5-b']dithiophene (**BDT-1**, linearly conjugated), benzo[1,2-b:4,5-b']dithiophene-4,8-dione (**BDT-2**, cross-conjugated with quinone), and benzo[1,2-b:5,4-b']dithiophene (**BDT-3**, cross-conjugated and an isomer of **BDT-1**). These compounds separate the influence of cross-conjugation (bond topology) from that of the electron-withdrawing effects of the quinone functionality while controlling for molecular formula and length. We investigated the charge transport properties of these molecules in tunneling junctions comprising self-assembled monolayers (SAMs), which are relevant for solid-state molecular-electronic devices.<sup>[47–49]</sup> Through a combination of density functional theory (DFT) and transition voltage spectroscopy (TVS) we show that cross-conjugation produces QI features near occupied molecular states and that the position and depth of the QI feature is strongly influenced by the strongly electron-withdrawing quinone functionality, which places these features near unoccupied states while simultaneously bringing those states close to  $E_F$ . Thus, by controlling bond topology and electronegativity separately, the conductance can be tuned independently of length and connectivity via the relative positions of the QI features and molecular states and not just the presence or absence of such features.

## RESULTS AND DISCUSSION

To isolate molecular effects on transport, it is important to control for changes to the width of the tunneling barrier which, in SAMs, is typically defined by the end-to-end lengths of the molecules. Conductance  $G$  generally varies exponentially with the barrier-width  $d$  such that  $G = G_0 \exp(-\beta d)$ , where  $G_0$  is the theoretical value of  $G$  when  $d = 0$ , and  $\beta$  is the tunneling decay coefficient. Since  $\beta$  depends on the positions of molecular states relative to



$E_F$  and we are comparing compounds with very different redox potentials (orbital energies) we can only ascribe changes to  $G$  if  $d$  is invariant across the series. Furthermore, to isolate the variable of bond topology experimentally, the electronic properties of the linear- and cross-conjugated compounds must be nearly identical. Figure 1a shows the structures of the **BDT- $n$**  series and **AQ**; the “arms” are linearly-conjugated phenylacetylenes (highlighted in the light blue background) and the cores (Ar, highlighted in the brown background) are substituted by the structures indicated. The variation in the end-to-end lengths of these compounds is within 1 Å and the linear- and cross-conjugated compounds **BDT-1** and **BDT-3** differ only by the relative position of sulfur atoms; they have the same molecular formula. The synthesis, full characterization and a detailed discussion of their properties are provided in the Supplementary Information. Note that we include **AQ** in the series as a benchmark for destructive QI effects.

We measured tunneling charge transport through metal-molecule-metal junctions comprising **BDT-1**, **BDT-2**, **BDT-3** and **AQ** using conformal eutectic Ga-In (EGaIn) contacts as top electrodes.<sup>[50]</sup> We utilized an established procedure of the *in situ* deprotection of thioacetates<sup>[41,51]</sup> to form well-defined SAMs on Au substrates; these substrates served then as bottom electrodes. We refer to the assembled junctions as Au/SAM//EGaIn where “/” and “//” denote a covalent and van der Waals interfaces, respectively. The geometry of the junctions is shown in Figure 1b. To verify that the structural similarities of the compounds carry over into the self-assembly process, we characterized the SAMs of **BDT- $n$**  by several complementary techniques, including (high-resolution) X-ray photoelectron spectroscopy (HRXPS/XPS) and angle-resolved near-edge X-ray absorption fine structure spectroscopy (NEXAFS). These data are discussed in detail in the Supplementary Information and summarized in Table 1. The characterization of SAMs of **AQ** is reported elsewhere.<sup>[16,41]</sup> The XPS and NEXAFS data suggest that the molecules in the **BDT- $n$**  SAMs are assembled upright with the tilt angle of approximately 35°. The molecules are packed densely on the order of  $10^{14}$  molecules per  $\text{cm}^2$  as are similar conjugated molecular-wire compounds.<sup>[41]</sup>



Figure 2a shows the current-density versus voltage ( $J/V$ ) curves for the **BDT- $n$**  series and **AQ** using EGaIn top contacts. **BDT-1** is the most conductive across the entire bias window. The conductance of linearly-conjugated **BDT-1** and **AC** (Figure S1; a linearly-conjugated analog of **AQ**), are almost identical (Figure S21), meaning that the low-bias conductivity and/or values of  $J$  are directly comparable between the **AC/AQ** and **BDT- $n$**  series. As expected, the cross-conjugated **BDT-2**, **BDT-3** and **AQ** are all less conductive than **BDT-1** (and **AC**). The low-bias conductivity (from the Ohmic region,  $-0.1$  V to  $0.1$  V) of the quinones (**BDT-2** and **AQ**), however, is even more suppressed than the cross-conjugated **BDT-3**, while the magnitudes of  $J$  for **BDT-2**, **BDT-3** and **AQ** are similar beyond  $-0.5$  V. We observed similar behavior in QI mediated by through-space conjugation in which the compound with an interference feature very close to  $E_F$  exhibited a sharp rise in  $J$ , eventually crossing  $J/V$  curve of the compound with a feature further from  $E_F$ .<sup>[41]</sup> This observation suggests that, as the junction is biased, the transmission probability “climbs” the interference feature rapidly, bringing highly transmissive conduction channels into the bias window at sufficiently low values of  $V$  to meet and exceed the total transmission of the compound for which the interference feature is far from  $E_F$  at zero bias. Further discussion on the asymmetry of  $J/V$  curves is included in the Supplementary Information.

To better compare the conductance of the molecules, we calculated the low-bias conductivities and normalized them to **BDT-1**. These values are plotted in Figure 2b, showing that cross-conjugation lowers the conductance of **BDT-3** by an order of magnitude compared to **BDT-1** and the quinone functionality of **BDT-2** and **AQ** lowers it by two orders of magnitude, in agreement with the analogous behavior of **AC** and **AQ**.<sup>[20]</sup> To control for large-area effects (*e.g.*, if there are defects in the SAM), we measured **BDT- $n$**  series by conducting-probe atomic force microscopy (CP-AFM) with Au electrodes and found the same trend: **BDT-1** > **BDT-3** > **BDT-2**, however, a direct comparison of low-bias conductivities was precluded by the extremely high resistance of **BDT-2** and **AQ** at low bias. These data are discussed in detail in the Supplementary Information. Thus, we conclude



that quinones suppress conductance more than cross-conjugation alone, irrespective of the measurement/device platform.

For insight into the shapes of the  $J/V$  curves and the conductance, we simulated the transmission spectra,  $T(E)$  vs.  $E - E_F$  ( $E_F$  value of  $-4.3$  eV, see Experimental Section), of the **BDT- $n$**  series using density functional theory (DFT) and compared the resulting curves with **AQ** (Figure 3). These calculations, which are discussed in more detail in the Computational Methodology section of the Supplementary Information, simulate the transmission spectra through isolated molecules in vacuum at zero bias and are useful for predicting trends in conductance. There are three important features of these curves: 1) Only the compounds with cross-conjugation (including quinones) show sharp dips (anti-resonances or QI features)<sup>[13,18]</sup> in the frontier orbital gap; 2) the dips occur near  $E_F$  only for the two quinones; and 3) the QI features are more pronounced for the molecules in which the cross-conjugation is caused by a quinone moiety as opposed to the carbon-carbon bond topology. When bias is applied to a junction, the x-axis of the transmission plot shifts and  $E_F$  broadens such that an integral starting at  $E - E_F = 0$  eV and widening to larger ranges of  $E - E_F$  is a rough approximation of how  $T(E)$  translates into current,  $I(V)$ . This relationship is apparent in the slightly lower conductance of **AQ** compared to **BDT-2** (Figure 2b) and the slightly lower values of  $T(E)$  for **AQ** compared to **BDT-2** across the entire range of  $E - E_F$ . The proximities of the QI features to  $E_F$  is also apparent in the  $J/V$  curves (Figure 2a). As the junction is biased, the minimum of the QI feature shifts such that, by 0.5 V, the transmission probabilities are roughly equal for **BDT- $n$**  and **AQ**.

The shape of  $T(E)$  near  $E - E_F = 0$  eV is roughly traced by differential conductance plots of  $\log | \frac{dJ}{dV} |$  vs.  $V$ , allowing QI features near  $E_F$  to be resolved experimentally.<sup>[18,41,52]</sup> Figure 4 shows heatmap plots of differential conductance of Au/SAM//EGaIn constructed from histograms binned to  $\log | \frac{dJ}{dV} |$  for each value of  $V$ . (Note that these are histograms of  $J/V$  curves with no data-selection, thus, brighter colors correspond to mean values of  $J$  and are not related to conductance histograms of single-molecule break-junctions; see





Supplementary Information for details.) Both **BDT-1** and **BDT-3** exhibit ordinary, U-shaped plots characteristic of non-resonant tunneling. By contrast, both **AQ** and **BDT-2**—the two compounds bearing quinone functionality—show V-shaped plots with negative curvature. These results are in agreement with Figure 3, which places the QI features for the quinone moieties, **AQ** and **BDT-2**, much closer to  $E_F$  than for **BDT-3**. The positions of these features are related to the positions of highest-occupied and lowest-unoccupied  $\pi$ -states (HOPS and LUPS), which are in good agreement between DFT and experiment (Tables S2 and S3). Thus, the differential conductance heatmaps (experiment) and DFT (simulation) both indicate that cross-conjugation suppresses conductance because it creates a dip in  $T(E)$  in the frontier orbital gap, but that the electron-withdrawing nature of the quinone functionality simultaneously pulls the LUPS and the interference features close to  $E_F$  such that the  $J/V$  characteristics and transmission plots of **AQ** and **BDT-2** are nearly indistinguishable despite the presence of two thienyl groups in **BDT-2**. These results also suggest that tunneling transport is mediated by the HOPS (hole-assisted tunneling) for **BDT-1** and **BDT-3** and by the LUPS (electron-assisted tunneling) for **BDT-2** and **AQ** because tunneling current is dominated by the resonance(s) closest to  $E_F$ .

To further investigate the mechanism of transport, we measured transition voltages,  $V_{\text{trans}}$  (Table S3, Figures S17 and S18), which provide information about the energy offset between  $E_F$  and the dominant frontier orbital.<sup>[53,54]</sup> Figure 5a shows the levels for the **BDT-*n*** series calculated by DFT with respect to  $E_F$  (−4.3 eV), clearly predicting LUPS-mediated tunneling for **BDT-2** and **AQ**. Figure 5b compares the experimental values of  $V_{\text{trans}}$  to the energy differences between  $E_F$  and the frontier orbitals. The salient feature of Figure 5b is that the trend in  $|E_{\text{HOPS}} - E_F|$  opposes the trend in  $V_{\text{trans}}$  such that the trend in experimental values of  $V_{\text{trans}}$  agrees with DFT only when we compare  $V_{\text{trans}}$  with  $|E_{\text{HOPS}} - E_F|$  for **BDT-1** and **BDT-3**, and with  $|E_{\text{LUPS}} - E_F|$  for **BDT-2** and **AQ**. Thus, DFT calculations combined with experimental values of  $V_{\text{trans}}$  predict electron-assisted tunneling for **BDT-2** and **AQ**. This degree of internal consistency between the experiment and theory is important



because, ultimately, the only primary observable is conductance, which we plot as  $J/V$  curves, differential conductance heatmaps and Fowler-Nordheim plots (from which we extract  $V_{\text{trans}}$ ). And we find remarkable agreement between these direct and indirect observations and DFT calculations on model junctions comprising single molecules.

## CONCLUSION

The key question of this work is how cross-conjugation and electronegativity affect QI features.<sup>[11,20,52,55,56]</sup> Based on our experimental observations and calculations, we assert that destructive QI induced by cross-conjugation is highly sensitive to the functional groups that induce the cross-conjugation and that quinones are, therefore, a poor testbed for tuning QI effects (beyond switching them on and off<sup>[57]</sup>) because their strong electron-withdrawing nature places a deep, destructive feature near  $E_F$  irrespective of other functional groups (in our case, two fused thiophene rings barely make a difference). Comparing a quinone to a hydrocarbon also compares HOPS-mediated tunneling to LUPS-mediated tunneling between molecules with significantly different band-gaps and absolute frontier orbital energies. In contrast, **BDT-1** and **BDT-3** are heterocyclic isomers with no functional groups, identical molecular formulas, nearly-identical HOPS, identical lengths that translate into SAMs of identical thicknesses, and transport is dominated by the HOPS. They isolate the single variable of conjugation patterns, allowing us to separate bond topology (cross-conjugation) from electronic properties (functional groups), giving experimental and theoretical insight into the relationship between bond topology and QI. Our results suggest that there is a lot of room to tune the conductance of moieties derived from **BDT-3** by including pendant groups (*e.g.*, halogens,  $\text{CF}_3$  groups or acidic/basic sites) that shift the QI feature gradually towards  $E_F$  synthetically and/or in response to chemical signals.



## Experimental

### Synthesis

**Reagents.** All reagents and solvents were commercial and were used as received. Benzo[1,2-b;4,5-b']dithiophene was purchased from TCI. 2,6-dibromobenzo[1,2-b:4,5-b']dithiophene-4,8-dione<sup>[58]</sup>, 2,6-dibromobenzo[1,2-b:5,4-b']dithiophene<sup>[59]</sup>, 4-ethynyl-1-thioacetylbenzene<sup>[60]</sup> and 1-tert-butylthio-4-ethynylbenzene<sup>[61]</sup> were synthesized according to literature procedures.

**NMR and Mass Spectra.** <sup>1</sup>HNMR and <sup>13</sup>CNMR were performed on a Varian Unity Plus (400 MHz) instrument at 25 °C, using tetramethylsilane (TMS) as an internal standard. NMR shifts are reported in ppm, relative to the residual protonated solvent signals of CDCl<sub>3</sub> ( $\delta$  = 7.26 ppm) or at the carbon absorption in CDCl<sub>3</sub> ( $\delta$  = 77.0 ppm). Multiplicities are denoted as: singlet (s), doublet (d), triplet (t) and multiplet (m). High Resolution Mass Spectroscopy (HRMS) was performed on a JEOL JMS 600 spectrometer.

**UV-Vis and Cyclic Voltammetry** UV-Vis measurements were carried out on a Jasco V-630 spectrometer. Cyclic voltammetry (CV) was carried out with a Autolab PGSTAT100 potentiostat in a three-electrode configuration.

**General.** Unless stated otherwise, all crude compounds were isolated by bringing the reaction to room temperature, extracting with CH<sub>2</sub>Cl<sub>2</sub>, washing with saturated NaHCO<sub>3</sub>, water and then brine. The organic phase was then collected and dried over Na<sub>2</sub>SO<sub>4</sub> and the solvents removed by rotary evaporation. Synthetic schemes and NMR spectra are provided in the Supplementary Information.

**2,6-dibromobenzo[1,2-b:4,5-b']dithiophene (1).** Benzo[1,2-b;4,5-b']dithiophene (540 mg, 2.84 mmol) were dissolved in 70 mL anhydrous THF under an atmosphere of N<sub>2</sub>, cooled to –78 °C and *n*-butyllithium (8.5 mmol, 5.3 mL, 1.6 M in hexane) was added drop-wise. The solution was stirred for 30 min in the cold bath before being warmed to room temperature and stirred for and additional 20 min. The mixture was cooled to –78 °C again and a solution



of CBr<sub>4</sub> (2.8 g, 8.5 mmol) in 5 mL anhydrous THF was added. The solution was stirred for 30 min in the cold bath before being quenched with concentrated sodium bicarbonate solution (10 mL) at  $-78^{\circ}\text{C}$ . The crude solid was purified by recrystallization from CHCl<sub>3</sub> to give **1** (890 mg, 90 %) as colorless platelets. <sup>1</sup>HNMR (400 MHz, CDCl<sub>3</sub>)  $\delta$ : 8.03 (s, 2H); 7.33 (s, 2H). <sup>13</sup>CNMR (100 MHz, CDCl<sub>3</sub>)  $\delta$ : 138.36, 136.88, 125.63, 116.00, 115.10.

**2,6-Bis[(4-acetylthiophenyl)ethynyl]benzo[1,2-b:4,5-b']dithiophene (BDT-1).** 2,6-dibromobenzo[1,2-b:4,5-b']dithiophene (125 mg, 0.36 mmol) and 4-ethynyl-1-thioacetylbenzene (176 mg, 1 mmol) were dissolved in mixture of fresh distilled Et<sub>3</sub>N (5 mL) and anhydrous THF (10 mL). After degassing with dry N<sub>2</sub>, the catalysts Pd(PPh<sub>3</sub>)<sub>4</sub> (58 mg, 0.05 mmol) and CuI (10 mg, 0.05 mmol) were added. The reaction mixture was refluxed overnight under N<sub>2</sub>. The crude solid was purified by column chromatography to give **BDT-1** (78 mg, 40 %). <sup>1</sup>HNMR (400 MHz, CDCl<sub>3</sub>)  $\delta$ : 8.17 (s, 2H), 7.59 (d, J=8.2, 4H), 7.55 (s, 2H), 7.43 (d, J=8.2, 4H), 2.45 (s, 6H). <sup>13</sup>CNMR (100 MHz, CDCl<sub>3</sub>)  $\delta$ : 195.88, 140.66, 140.46, 136.90, 134.76, 131.51, 130.89, 126.53, 126.25, 119.27, 97.57, 87.31, 32.97. HRMS(ESI) calcd. for C<sub>30</sub>H<sub>18</sub>O<sub>2</sub>S<sub>4</sub> [M+H]<sup>+</sup>: 539.02624, found: 539.02457.

**2,6-Bis[(4-tert-butylthiophenyl)ethynyl]benzo[1,2-b:4,5-b']dithiophene-4,8-dione (5).** 2,6-dibromobenzo[1,2-b:4,5-b']dithiophene-4,8-dione (**3**; 200 mg, 0.53 mmol) and 1-tert-butylthio-4-ethynylbenzene (**4**; 230 mg, 1.21 mmol) were dissolved in mixture of fresh distilled Et<sub>3</sub>N (5 mL) and anhydrous THF (10 mL). After degassing, the catalysts Pd(PPh<sub>3</sub>)<sub>4</sub> (30 mg, 0.03 mmol) and CuI (5 mg, 0.03 mmol) were added. The reaction mixture was refluxed for overnight under N<sub>2</sub>. The crude solid was purified by column chromatography to give **5** (100 mg, 32 %). <sup>1</sup>HNMR (400 MHz, CDCl<sub>3</sub>)  $\delta$ : 7.71 (s, 2H), 7.55 (d, J=8.2, 4H), 7.50 (d, J=8.2, 4H), 1.31 (s, 18H). <sup>13</sup>CNMR (100 MHz, CDCl<sub>3</sub>)  $\delta$ : 173.33, 143.91, 142.55, 137.24, 135.17, 131.73, 131.56, 130.31, 121.70, 98.14, 82.55, 46.81, 31.02.

**2,6-Bis[(4-acetylthiophenyl)ethynyl]benzo[1,2-b:4,5-b']dithiophene-4,8-dione (BDT-2).** [62] TiCl<sub>4</sub> (0.04 mL, 0.364 mmol) was added drop-wise to a solution of compound **5** (100 mg, 0.167 mmol) and CH<sub>3</sub>C(O)Cl (0.03 mL, 0.377 mmol) in CH<sub>2</sub>Cl<sub>2</sub> at 0  $^{\circ}\text{C}$ . The resulting mix-



ture was stirred at room temperature for 1 h and the conversion was monitored by TLC (hexanes/ $\text{CH}_2\text{Cl}_2$ , 2:1). Upon completion, the reaction was quenched with water (10 mL). The crude solid was purified by column chromatography to give **BDT-2** (50 mg, 53 %).  $^1\text{H}$ NMR (400 MHz,  $\text{CDCl}_3$ )  $\delta$ : 7.73 (s, 2H), 7.59 (d,  $J=8.2$ , 4H), 7.45 (d,  $J=8.2$ , 4H), 2.46 (s, 6H).  $^{13}\text{C}$ NMR (100 MHz,  $\text{CDCl}_3$ )  $\delta$ : 195.59, 175.96, 145.20, 136.95, 134.87, 134.20, 133.15, 132.57, 132.50, 125.24, 100.42, 85.49, 33.01. HRMS(ESI) calcd. for  $\text{C}_{30}\text{H}_{17}\text{O}_4\text{S}_4$   $[\text{M}+\text{H}]^+$ : 569,00042, found: 568.99887.

**2,6-Bis[(4-tert-butylthiophenyl)ethynyl]benzo[1,2-b:5,4-b']dithiophene (7).** 2,6-dibromobenzo[1,2-b:5,4-b']dithiophene (**6**; 50 mg, 0.143 mmol) and 1-tert-butylthio-4-ethynylbenzene (**4**; 68 mg, 0.358 mmol) were dissolved in mixture of fresh distilled  $\text{Et}_3\text{N}$  (5 mL) and anhydrous THF (10 mL). After degassing, the catalysts  $\text{Pd}(\text{PPh}_3)_4$  (16 mg, 0.014 mmol) and  $\text{CuI}$  (2.7 mg, 0.014 mmol) were added. The reaction mixture was refluxed overnight under  $\text{N}_2$ . The crude solid was purified by column chromatography to give **7** (40 mg, 49 %).  $^1\text{H}$ NMR (400 MHz,  $\text{CDCl}_3$ )  $\delta$ : 8.16 (s, 1H), 8.14 (s, 1H), 7.56 (s, 2H), 7.54 (d,  $J=4$ , 4H), 7.51 (d,  $J=4$ , 4H), 1.31 (s, 18H).  $^{13}\text{C}$ NMR (100 MHz,  $\text{CDCl}_3$ )  $\delta$ : 141.35, 140.05, 139.89, 136.77, 134.10, 131.29, 125.64, 125.38, 120.85, 117.39, 97.51, 86.99, 49.30, 33.67.

**2,6-Bis[(4-acetylthiophenyl)ethynyl]benzo[1,2-b:5,4-b'] dithiophene (BDT-3).**<sup>[62]</sup>  $\text{TiCl}_4$  (0.042 mL, 0.388 mmol) was added drop-wise to a solution of compound (**7**) (100 mg, 0.176 mmol) and  $\text{CH}_3\text{C}(\text{O})\text{Cl}$  (0.03 mL, 0.397 mmol) in  $\text{CH}_2\text{Cl}_2$  at  $0^\circ\text{C}$ . The resulting mixture was stirred at room temperature for 10 min and the conversion was monitored by TLC (hexanes/ $\text{CH}_2\text{Cl}_2$  2:1). Upon completion the reaction was quenched with water (10 mL). The crude solid was purified by column chromatography to give **BDT-3** (25 mg, 26 %).  $^1\text{H}$ NMR (400 MHz,  $\text{CDCl}_3$ )  $\delta$ : 8.17 (s, 1H), 8.15 (s, 1H), 7.59 (d,  $J=7.2$ , 4H), 7.58 (s, 2H), 7.43 (d,  $J=8.2$ , 4H), 2.45 (s, 3H).  $^{13}\text{C}$ NMR (100 MHz,  $\text{CDCl}_3$ )  $\delta$ : 195.88, 141.43, 140.03, 136.90, 134.76, 131.51, 131.48, 126.27, 126.50, 120.94, 117.42, 97.22, 87.15, 32.97. HRMS(ESI) calcd. for  $\text{C}_{30}\text{H}_{18}\text{O}_2\text{S}_4$   $[\text{M}+\text{H}]^+$ : 539,02624, found: 539.02476.



## Self-assembled monolayers

The SAMs of **BDT-*n*** were formed via *in situ* deprotection<sup>[41,51]</sup> on template-stripped Au substrates.<sup>[63]</sup> Freshly template-stripped substrates were immersed into 3 mL of 50  $\mu$ M solutions of the thioacetate precursors in freshly distilled toluene inside a nitrogen-filled glovebox and sealed under a nitrogen atmosphere. The sealed vessels were kept inside a nitrogen flow box<sup>[64]</sup> ( $O_2$  below 3 %, RH below 15 %) overnight; all subsequent handling and EGaIn measurements were performed inside the flowbox. 1.5 h prior to measurement, 0.05 mL of 17 mM diazabicycloundec-7-ene (DBU) in toluene was added to the precursor/substrate solution. The substrates were then rinsed with toluene and allowed to dry for 30 min before performing the measurements.

## Characterization

The SAMs of **BDT-*n*** were characterized by XPS (laboratory and synchrotron), NEXAFS spectroscopy, UPS and water contact angles. In some cases, SAMs of  $CH_3(CH_2)_{15}SH$  or  $CH_3(CH_2)_{17}SH$  on Au were used as a reference. See Supplementary Information for details.

## Transport measurements

**EGaIn.** For each SAM, at least 10 junctions were measured on each of three different substrates by applying a bias from 0.00 V  $\rightarrow$  1.00 V  $\rightarrow$  -1.00 V  $\rightarrow$  0.00 V with steps of 0.05 V. At least 20 trace/re-trace cycles were measured for each junction; only junctions that did not short over all 20 cycles were counted as “working junction” for computing yields.

**CP-AFM.** *I-V* measurements were performed on a Bruker AFM Multimode MMAFM-2 equipped with a Peak Force TUNA Application Module. The Au on mica substrates were removed from the flowbox immediately prior to measurement, which occurred under ambient conditions by contacting the SAM with a Au-coated  $Si_3N_4$  tip with a nominal radius of 30 nm



(NPG-10, Bruker; resonant frequency: 65 kHz, spring constant: 0.35 N/m). The AFM tip was grounded and the samples were biased from  $-1.0\text{ V} \rightarrow 1.0\text{ V} \rightarrow -1.0\text{ V}$  on  $\text{Au}^{\text{Mica}}$ . 11 trace/re-trace cycles per junction were performed and the top electrode was removed from SAMs between junctions.

**Processing.** All raw data were processed algorithmically using Scientific Python to generate histograms, Gaussian fits, extract transition voltages and construct differential conductance heatmap plots.

## DFT calculations

Calculations were performed using the ORCA 4 software package<sup>[65,66]</sup> and the ARTAIOS-030417 software package.<sup>[67,68]</sup> The molecules terminating with thiols were first minimized to find the gas-phase geometry and then attached to two 18-atom Au(111) clusters via the terminal sulfur atoms with a distance of 1.75 Å at hexagonal close-pack hollow sites (hydrogen atom from the thiol was deleted before attaching the electrodes). Single-point energy calculations were performed on this model junction using B3LYP/G and LANL2DZ basis sets according to literature procedures to compute the energy levels.<sup>[67]</sup> Transmission curves and isoplots of the central molecular orbitals, for isolated molecules without electrodes and terminal hydrogen atoms, were generated using the ARTAIOS-030417 software package and the energy axis was scaled using the  $E_{\text{F}}$  of  $-4.3\text{ eV}$ . The use of this  $E_{\text{F}}$  value for comparing transmission trends to the experimental tunneling conduction in Au/SAM//EGaIn junction is supported by the UPS measurements that also give a similar  $E_{\text{F}}$  value (see Supplementary Information section 1.3.3). It has also been established experimentally that SAMs of aliphatic and conjugated molecules on Au shift the  $E_{\text{F}}$  values by 0.85 and 0.98 eV, respectively, (*i.e.*, to  $-4.2\text{ eV}$  to  $-4.4\text{ eV}$ ) from  $-5.2\text{ eV}$  for a clean gold surface.<sup>[69–71]</sup> This value of  $E_{\text{F}}$  was used for all DFT calculations. Further rationale for choosing this value of  $E_{\text{F}}$  and the detailed step-wise procedure for all the calculations involved is further described in Supplementary Information.



## ACKNOWLEDGMENTS

R.C.C., Y.Z. and M.C. acknowledge the European Research Council for the ERC Starting Grant 335473 (MOLECSYNCON). G.Y. acknowledges financial support from the China Scholarship Council (CSC):NO.201408440247. X.Q. acknowledges the Zernike Institute for Advanced Materials “Dieptestrategie.” E.S. and M.Z. thank the Helmholtz Zentrum Berlin for the allocation of synchrotron radiation beamtime at BESSY II and A. Nefedov and Ch. Wöll for the technical cooperation during the experiments there; a financial support of the German Research Society (Deutsche Forschungsgemeinschaft; DFG) within the grant ZH 63/22-1 is appreciated. We thank the Center for Information Technology of the University of Groningen for their support and for providing access to the Peregrine high performance computing cluster.





## References

1. Vilan, A.; Aswal, D.; Cahen, D. Large-Area, Ensemble Molecular Electronics: Motivation and Challenges. *Chem. Rev.* **2017**, *117*, 4248–4286.
2. Xin, N.; Guo, X. Catalyst: The Renaissance of Molecular Electronics. *Chem* **2017**, *3*, 373–376.
3. Lörtscher, E. Reaction: Technological Aspects of Molecular Electronics. *Chem* **2017**, *3*, 376–377.
4. Hsu, L.-Y.; Jin, B.-Y.; Chen, C.-h.; Peng, S.-M. Reaction: New Insights Into Molecular Electronics. *Chem* **2017**, *3*, 378–379.
5. Lambert, C. J. Basic Concepts of Quantum Interference and Electron Transport in Single-Molecule Electronics. *Chem. Soc. Rev.* **2015**, *44*, 875–888.
6. Webb, R. a.; Washburn, S.; Umbach, C. P.; Laibowitz, R. B. Observation of He Aharonov-Bohm Oscillations in Normal-Metal Rings. *Phys. Rev. Lett.* **1985**, *54*, 2696–2699.
7. Sautet, P.; Joachim, C. Electronic Interference Produced by a Benzene Embedded in a Polyacetylene Chain. *Chem. Phys. Lett.* **1988**, *153*, 511–516.
8. Hsu, L.-Y.; Jin, B.-Y. An investigation of quantum transport by the free-electron network model: Resonance and interference effects. *Chemical Physics* **2009**, *355*, 177–182.
9. Cardamone, D. M.; Stafford, C. A.; Mazumdar, S. Controlling Quantum Transport through a Single Molecule. *Nano Letters* **2006**, *6*, 2422–2426.
10. Solomon, G. C.; Andrews, D. Q.; Van Duyne, R. P.; Ratner, M. A. When Things Are Not as They Seem: Quantum Interference Turns Molecular Electron Transfer “Rules” Upside Down. *J. Am. Chem. Soc.* **2008**, *130*, 7788–7789.



11. Solomon, G. C.; Andrews, D. Q.; Goldsmith, R. H.; Hansen, T.; Wasielewski, M. R.; Van Duyne, R. P.; Ratner, M. a. Quantum Interference in Acyclic Systems: Conductance of Cross-Conjugated Molecules. *J. Am. Chem. Soc.* **2008**, *130*, 17301–17308.
12. Andrews, D. Q.; Solomon, G. C.; Goldsmith, R. H.; Hansen, T.; Wasielewski, M. R.; Duyne, R. P. V.; Ratner, M. A. Quantum Interference: The Structural Dependence of Electron Transmission Through Model Systems and Cross-Conjugated Molecules. *J. Phys. Chem. C* **2008**, *112*, 16991–16998.
13. Solomon, G. C.; Herrmann, C.; Hansen, T.; Mujica, V.; Ratner, M. A. Exploring Local Currents in Molecular Junctions. *Nat. Chem.* **2010**, *2*, 223–228.
14. Maggio, E.; Solomon, G. C.; Troisi, A. Exploiting Quantum Interference in Dye Sensitized Solar Cells. *ACS Nano* **2014**, *8*, 409–418.
15. Pedersen, K. G. L.; Borges, A.; Hedegård, P.; Solomon, G. C.; Strange, M. Illusory Connection Between Cross-Conjugation and Quantum Interference. *J. Phys. Chem. C* **2015**, *119*, 26919–26924.
16. Fracasso, D.; Valkenier, H.; Hummelen, J. C.; Solomon, G. C.; Chiechi, R. C. Evidence for Quantum Interference in SAMs of Arylethynylene Thiolates in Tunneling Junctions With Eutectic Ga-In (EGaIn) Top-Contacts. *J. Am. Chem. Soc.* **2011**, *133*, 9556–9563.
17. Hong, W.; Valkenier, H.; Mészáros, G.; Manrique, D. Z.; Mishchenko, A.; Putz, A.; García, P. M.; Lambert, C. J.; Hummelen, J. C.; Wandlowski, T. An MCBJ Case Study: The Influence of  $\Pi$ -Conjugation on the Single-Molecule Conductance at a Solid/Liquid Interface. *Beilstein J. Nanotechnol.* **2011**, *2*, 699–713.
18. Guedon, C. M.; Valkenier, H.; Markussen, T.; Thygesen, K. S.; Hummelen, J. C.; Van Der Molen, S. J. Observation of Quantum Interference in Molecular Charge Transport. *Nat. Nanotechnol.* **2012**, *7*, 305–309.



19. Kaliginedi, V.; Moreno-García, P.; Valkenier, H.; Hong, W.; García-Suárez, V. M.; Buiter, P.; Otten, J. L. H.; Hummelen, J. C.; Lambert, C. J.; Wandlowski, T. Correlations Between Molecular Structure and Single-Junction Conductance: A Case Study With Oligo(phenylene-Ethynylene)-Type Wires. *J. Am. Chem. Soc.* **2012**, *134*, 5262–5275.
20. Valkenier, H.; Guedon, C. M.; Markussen, T.; Thygesen, K. S.; van der Molen, S. J.; Hummelen, J. C. Cross-Conjugation and Quantum Interference: A General Correlation? *Phys. Chem. Chem. Phys.* **2014**, *16*, 653–662.
21. Koole, M.; Thijssen, J. M.; Valkenier, H.; Hummelen, J. C.; van der Zant, H. S. J. Electric-Field Control of Interfering Transport Pathways in a Single-Molecule Anthraquinone Transistor. *Nano Lett.* **2015**, *15*, 5569–5573.
22. Bergfield, J. P.; Heitzer, H. M.; Van Dyck, C.; Marks, T. J.; Ratner, M. A. Harnessing Quantum Interference in Molecular Dielectric Materials. *ACS Nano* **2015**, *9*, 6412–6418.
23. Markussen, T.; Stadler, R.; Thygesen, K. S. The Relation Between Structure and Quantum Interference in Single Molecule Junctions. *Nano Lett.* **2010**, *10*, 4260–4265.
24. Salhani, C.; Della Rocca, M. L.; Bessis, C.; Bonnet, R.; Barraud, C.; Lafarge, P.; Chevilot, A.; Martin, P.; Lacroix, J. C. Inelastic Electron Tunneling Spectroscopy in Molecular Junctions Showing Quantum Interference. *Phys. Rev. B* **2017**, *95*, 165431.
25. Mayor, M.; Weber, H. B.; Reichert, J.; Elbing, M.; von Hänisch, C.; Beckmann, D.; Fischer, M. Electric Current Through a Molecular Rod—Relevance of the Position of the Anchor Groups. *Angew. Chem., Int. Ed.* **2003**, *42*, 5834–5838.
26. Taniguchi, M.; Tsutsui, M.; Mogi, R.; Sugawara, T.; Tsuji, Y.; Yoshizawa, K.; Kawai, T. Dependence of Single-Molecule Conductance on Molecule Junction Symmetry. *J. Am. Chem. Soc.* **2011**, *133*, 11426–11429.



27. Meisner, J. S.; Ahn, S.; Aradhya, S. V.; Krikorian, M.; Parameswaran, R.; Steigerwald, M.; Venkataraman, L.; Nuckolls, C. Importance of Direct Metal $\pi$  Coupling in Electronic Transport Through Conjugated Single-Molecule Junctions. *J. Am. Chem. Soc.* **2012**, *134*, 20440–20445.
28. Arroyo, C. R.; Tarkuc, S.; Frisenda, R.; Seldenthuis, J. S.; Woerde, C. H. M.; Eelkema, R.; Grozema, F. C.; van der Zant, H. S. J. Signatures of Quantum Interference Effects on Charge Transport Through a Single Benzene Ring. *Angew. Chem., Int. Ed.* **2013**, *52*, 3152–3155.
29. Quinn, J. R.; Foss, F. W.; Venkataraman, L.; Hybertsen, M. S.; Breslow, R. Single-Molecule Junction Conductance Through Diaminoacenes. *J. Am. Chem. Soc.* **2007**, *129*, 6714–6715.
30. Kiguchi, M.; Nakamura, H.; Takahashi, Y.; Takahashi, T.; Ohto, T. Effect of Anchoring Group Position on Formation and Conductance of a Single Disubstituted Benzene Molecule Bridging Au Electrodes: Change of Conductive Molecular Orbital and Electron Pathway. *J. Phys. Chem. C* **2010**, *114*, 22254–22261.
31. Aradhya, S. V.; Meisner, J. S.; Krikorian, M.; Ahn, S.; Parameswaran, R.; Steigerwald, M. L.; Nuckolls, C.; Venkataraman, L. Dissecting Contact Mechanics From Quantum Interference in Single-Molecule Junctions of Stilbene Derivatives. *Nano Lett.* **2012**, *12*, 1643–1647.
32. Manrique, D. Z.; Huang, C.; Baghernejad, M.; Zhao, X.; Al-Owaedi, O. a.; Sadeghi, H.; Kaliginedi, V.; Hong, W.; Gulcur, M.; Wandlowski, T. *et al.* A Quantum Circuit Rule for Interference Effects in Single-Molecule Electrical Junctions. *Nat. Commun.* **2015**, *6*, 6389.
33. Xia, J.; Capozzi, B.; Wei, S.; Strange, M.; Batra, A.; Moreno, J. R.; Amir, R. J.;



- Amir, E.; Solomon, G. C.; Venkataraman, L. *et al.* Breakdown of Interference Rules in Azulene, a Nonalternant Hydrocarbon. *Nano Lett.* **2014**, *14*, 2941–2945.
34. Schwarz, F.; Koch, M.; Kastlunger, G.; Berke, H.; Stadler, R.; Venkatesan, K.; Lörtscher, E. Charge Transport and Conductance Switching of Redox-Active Azulene Derivatives. *Angew. Chem., Int. Ed.* **2016**, *55*, 11781–11786.
35. Yang, G.; Sangtarash, S.; Liu, Z.; Li, X.; Sadeghi, H.; Tan, Z.; Li, R.; Zheng, J.; Dong, X.; Liu, J.-Y. *et al.* Protonation Tuning of Quantum Interference in Azulene-Type Single-Molecule Junctions. *Chem. Sci.* **2017**, *8*, 7505–7509.
36. Baer, R.; Neuhauser, D. Phase Coherent Electronics: A Molecular Switch Based on Quantum Interference. *J. Am. Chem. Soc.* **2002**, *124*, 4200–4201.
37. Solomon, G. C.; Herrmann, C.; Vura-Weis, J.; Wasielewski, M. R.; Ratner, M. A. The Chameleonic Nature of Electron Transport Through  $\Pi$ -Stacked Systems. *J. Am. Chem. Soc.* **2010**, *132*, 7887–7889.
38. Kocherzhenko, A. A.; Grozema, F. C.; Siebbeles, L. D. A. Charge Transfer Through Molecules With Multiple Pathways: Quantum Interference and Dephasing. *J. Phys. Chem. C* **2010**, *114*, 7973–7979.
39. Phelan, N. F.; Orchin, M. Cross Conjugation. *J. Chem. Educ.* **1968**, *45*, 633–637.
40. Limacher, P. a.; Lüthi, H. P. Cross-Conjugation. *Wiley Interdiscip. Rev.: Comput. Mol. Sci.* **2011**, *1*, 477–486.
41. Carlotti, M.; Kovalchuk, A.; Wächter, T.; Qiu, X.; Zharnikov, M.; Chiechi, R. C. Conformation-Driven Quantum Interference Effects Mediated by Through-Space Conjugation in Self-Assembled Monolayers. *Nat. Commun.* **2016**, *7*, 13904.



42. Borges, A.; Xia, J.; Liu, S. H.; Venkataraman, L.; Solomon, G. C. The Role of Through-Space Interactions in Modulating Constructive and Destructive Interference Effects in Benzene. *Nano Lett.* **2017**, *17*, 4436–4442.
43. Sangtarash, S.; Sadeghi, H.; Lambert, C. J. Exploring Quantum Interference in Heteroatom-Substituted Graphene-Like Molecules. *Nanoscale* **2016**, *8*, 13199–13205.
44. Liu, X.; Sangtarash, S.; Reber, D.; Zhang, D.; Sadeghi, H.; Shi, J.; Xiao, Z.-Y.; Hong, W.; Lambert, C. J.; Liu, S.-X. Gating of Quantum Interference in Molecular Junctions by Heteroatom Substitution. *Angew. Chem., Int. Ed.* **2017**, *56*, 173–176.
45. Tsuji, Y.; Stuyver, T.; Gunasekaran, S.; Venkataraman, L. The Influence of Linkers on Quantum Interference: A Linker Theorem. *J. Phys. Chem. C* **2017**, *121*, 14451–14462.
46. Lissau, H.; Frisenda, R.; Olsen, S. T.; Jevric, M.; Parker, C. R.; Kadziola, A.; Hansen, T.; van der Zant, H. S. J.; Nielsen, M. B.; Mikkelsen, K. V. Tracking molecular resonance forms of donor–acceptor push–pull molecules by single-molecule conductance experiments. *Nat. Commun.* **2015**, *6*, 10233.
47. Wang, Z.; Dong, H.; Li, T.; Hviid, R.; Zou, Y.; Wei, Z.; Fu, X.; Wang, E.; Zhen, Y.; Norgaard, K. *et al.* Role of redox centre in charge transport investigated by novel self-assembled conjugated polymer molecular junctions. *Nat Commun* **2015**, *6*, 7478.
48. Pourhossein, P.; Vijayaraghavan, R. K.; Meskers, S. C. J.; Chiechi, R. C. Optical Modulation of Nano-Gap Tunnelling Junctions Comprising Self-Assembled Monolayers of Hemicyanine Dyes. *Nat. Commun.* **2016**, *7*, 11749.
49. Seo, S.; Hwang, E.; Cho, Y.; Lee, J.; Lee, H. Functional Molecular Junctions Derived From Double Self-Assembled Monolayers. *Angew. Chem., Int. Ed.* **2017**, *56*, 12122–12126.



50. Chiechi, R. C.; Weiss, E. A.; Dickey, M. D.; Whitesides, G. M. Eutectic Gallium–Indium (EGaIn): A Moldable Liquid Metal for Electrical Characterization of Self-Assembled Monolayers. *Angew. Chem., Int. Ed.* **2008**, *120*, 148–150.
51. Valkenier, H.; Huisman, E. H.; van Hal, P. A.; de Leeuw, D. M.; Chiechi, R. C.; Hummel, J. C. Formation of High-Quality Self-Assembled Monolayers of Conjugated Dithiols on Gold: Base Matters. *J. Am. Chem. Soc.* **2011**, *133*, 4930–4939.
52. Lykkebo, J.; Gagliardi, A.; Pecchia, A.; Solomon, G. C. IETS and Quantum Interference: Propensity Rules in the Presence of an Interference Feature. *J. Chem. Phys.* **2014**, *141*, 124119.
53. Beebe, J. M.; Kim, B.; Frisbie, C. D.; Kushmerick, J. G. Measuring Relative Barrier Heights in Molecular Electronic Junctions With Transition Voltage Spectroscopy. *ACS Nano* **2008**, *2*, 827–832.
54. Zhang, Y.; Qiu, X.; Gordiichuk, P.; Soni, S.; Krijger, T. L.; Herrmann, A.; Chiechi, R. C. Mechanically and Electrically Robust Self-Assembled Monolayers for Large-Area Tunneling Junctions. *J. Phys. Chem. C* **2017**, *121*, 14920–14928.
55. Pedersen, K. G. L.; Strange, M.; Leijnse, M.; Hedegard, P.; Solomon, G. C.; Paaske, J. Quantum Interference in Off-Resonant Transport Through Single Molecules. *Phys. Rev. B* **2014**, *90*, 125413.
56. Solomon, G. C. *Cross Conjugation*; Wiley-VCH Verlag GmbH & Co. KGaA, 2016; pp 397–412.
57. Baghernejad, M.; Zhao, X.; Baruël Ørnsø, K.; Füeg, M.; Moreno-García, P.; Rudnev, A. V.; Kaliginedi, V.; Vesztergom, S.; Huang, C.; Hong, W. *et al.* Electrochemical Control of Single-Molecule Conductance by Fermi-Level Tuning and Conjugation Switching. *J. Am. Chem. Soc.* **2014**, *136*, 17922–17925.



58. Kuo, C.-Y.; Nie, W.; Tsai, H.; Yen, H.-J.; Mohite, A. D.; Gupta, G.; Dattelbaum, A. M.; William, D. J.; Cha, K. C.; Yang, Y. *et al.* Structural Design of Benzo[1,2-B:4,5-B']dithiophene-Based 2D Conjugated Polymers With Bithienyl and Terthienyl Substituents Toward Photovoltaic Applications. *Macromolecules* **2014**, *47*, 1008–1020.
59. Rieger, R.; Beckmann, D.; Mavrinskiy, A.; Kastler, M.; Müllen, K. Backbone Curvature in Polythiophenes. *Chem. Mater.* **2010**, *22*, 5314–5318.
60. Shi, Z.-F.; Wang, L.-J.; Wang, H.; Cao, X.-P.; Zhang, H.-L. Synthesis of Oligo(phenylene Ethynylene)s With Dendrimer “Shells” for Molecular Electronics. *Org. Lett.* **2007**, *9*, 595–598.
61. van Dijk, E. H.; Myles, D. J. T.; van der Veen, M. H.; Hummelen, J. C. Synthesis and Properties of an Anthraquinone-Based Redox Switch for Molecular Electronics. *Org. Lett.* **2006**, *8*, 2333–2336.
62. Pijper, T. C.; Robertus, J.; Browne, W. R.; Feringa, B. L. Mild Ti-Mediated Transformation of T-Butyl Thio-Ethers Into Thio-Acetates. *Org. Biomol. Chem.* **2015**, *13*, 265–268.
63. Weiss, E. A.; Kaufman, G. K.; Kriebel, J. K.; Li, Z.; Schalek, R.; Whitesides, G. M. Si/SiO<sub>2</sub>-Templated Formation of Ultraflat Metal Surfaces on Glass, Polymer, and Solder Supports: Their Use as Substrates for Self-Assembled Monolayers. *Langmuir* **2007**, *23*, 9686–9694.
64. Carlotti, M.; Degen, M.; Zhang, Y.; Chiechi, R. C. Pronounced Environmental Effects on Injection Currents in EGaIn Tunneling Junctions Comprising Self-Assembled Monolayers. *J. Phys. Chem. C* **2016**, *120*, 20437–20445.
65. Neese, F. The ORCA Program System. *Wiley Interdiscip. Rev.: Comput. Mol. Sci.* **2012**, *2*, 73–78.





66. Neese, F. Software update: the ORCA program system, version 4.0. *Wiley Interdisciplinary Reviews: Computational Molecular Science*
67. Herrmann, C.; Gross, L.; Steenbock, T.; Deffner, M.; Voigt, B. A.; Solomon, G. C. ARTAIOS - A Transport Code for Postprocessing Quantum Chemical Electronic Structure Calculations, Available From <https://www.chemie.uni-hamburg.de/ac/herrmann/software/index.html>. 2016.
68. Herrmann, C.; Solomon, G. C.; Subotnik, J. E.; Mujica, V.; Ratner, M. A. Ghost Transmission: How Large Basis Sets Can Make Electron Transport Calculations Worse. *J. Chem. Phys.* **2010**, *132*, 024103.
69. Cabarcos, O. M.; Schuster, S.; Hehn, I.; Zhang, P. P.; Maitani, M. M.; Sullivan, N.; Gigure, J.-B.; Morin, J.-F.; Weiss, P. S.; Zojer, E. *et al.* Effects of Embedded Dipole Layers on Electrostatic Properties of Alkanethiolate Self-Assembled Monolayers. *The Journal of Physical Chemistry C* **2017**, *121*, 15815–15830.
70. AbuHusein, T.; Schuster, S.; Egger, D. A.; Kind, M.; Santowski, T.; Wiesner, A.; Chiechi, R.; Zojer, E.; Terfort, A.; Zharnikov, M. The Effects of Embedded Dipoles in Aromatic SelfAssembled Monolayers. *Advanced Functional Materials* *25*, 3943–3957.
71. Kovalchuk, A.; Abu-Husein, T.; Fracasso, D.; Egger, D. A.; Zojer, E.; Zharnikov, M.; Terfort, A.; Chiechi, R. C. Transition voltages respond to synthetic reorientation of embedded dipoles in self-assembled monolayers. *Chem. Sci.* **2016**, *7*, 781–787.



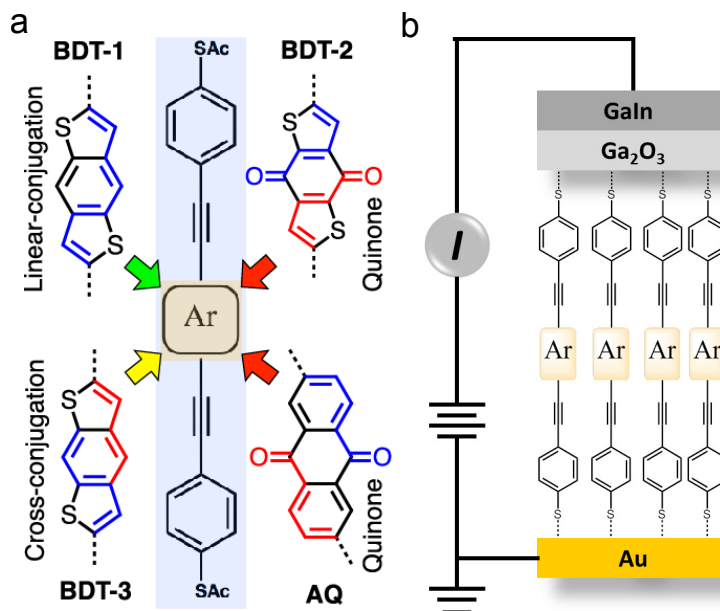


Figure 1: (a) Structures of **BDT-1**, **BDT-2** and **BDT-3** with linearly and cross-conjugated pathways of the cores drawn in blue and red, respectively. The phenylacetylene arms (highlighted in blue) are linearly conjugated. **BDT-1** is linearly-conjugated, **BDT-2** contains a cross-conjugation imposed by the central quinone ring analogous to **AQ** and **BDT-3** is similarly cross-conjugated, but the cross-conjugation separating the two linearly-conjugated pathways arises from the positions of the sulfur atoms relative to the central phenyl ring (there are no exocyclic bonds). (b) Schematic of Au/SAM//EGaIn junction (“//” and “//” denote a covalent and van der Waals interfaces, respectively).



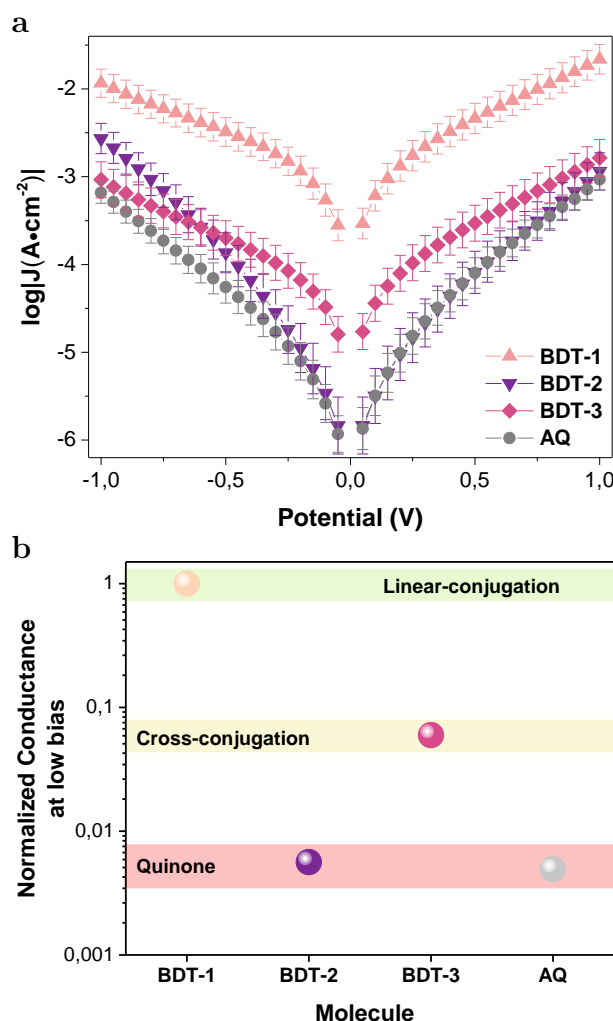


Figure 2: (a) Plots of  $\log |J(\text{A}\cdot\text{cm}^{-2})|$  versus  $V$  of Au/SAM//EGaIn junctions comprising SAMs of **BDT-1** (salmon up-triangles), **BDT-2** (purple down-triangles), **BDT-3** (pink diamonds) and **AQ** (grey circles). Each datum is the peak position of a Gaussian fit of  $\log |J|$  for that voltage. The error bars are 95 % confidence intervals taking each junction as a degree of freedom. (b) Normalized low bias conductance, linearly conjugated **BDT-1** (salmon ball) features the highest values, the quinone **BDT-2** (purple ball) and **AQ** (grey ball) the lowest and cross conjugated **BDT-3** (pink ball) is in between.



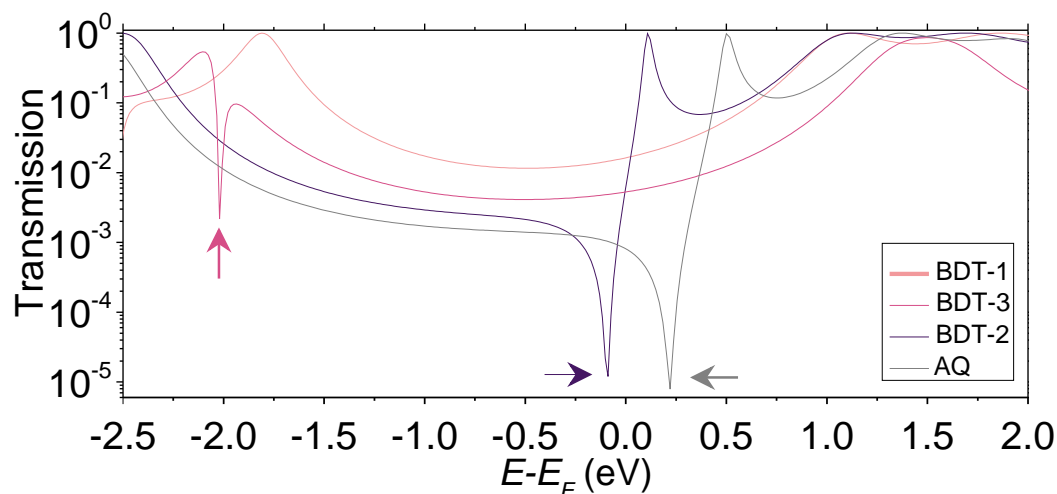


Figure 3: Transmission spectra for isolated molecules of **BDT-*n*** and **AQ**. The spectrum of **BDT-1** (salmon) is featureless between the resonances ( $T(E) \rightarrow 1$ ) near the frontier orbitals. The sharp dips in the spectra of **BDT-2** (purple), **BDT-3** (pink) and **AQ** (grey) indicated with arrows are destructive QI features. The energies on the bottom axis are with respect to the  $E_F$  value of  $-4.3$  eV.



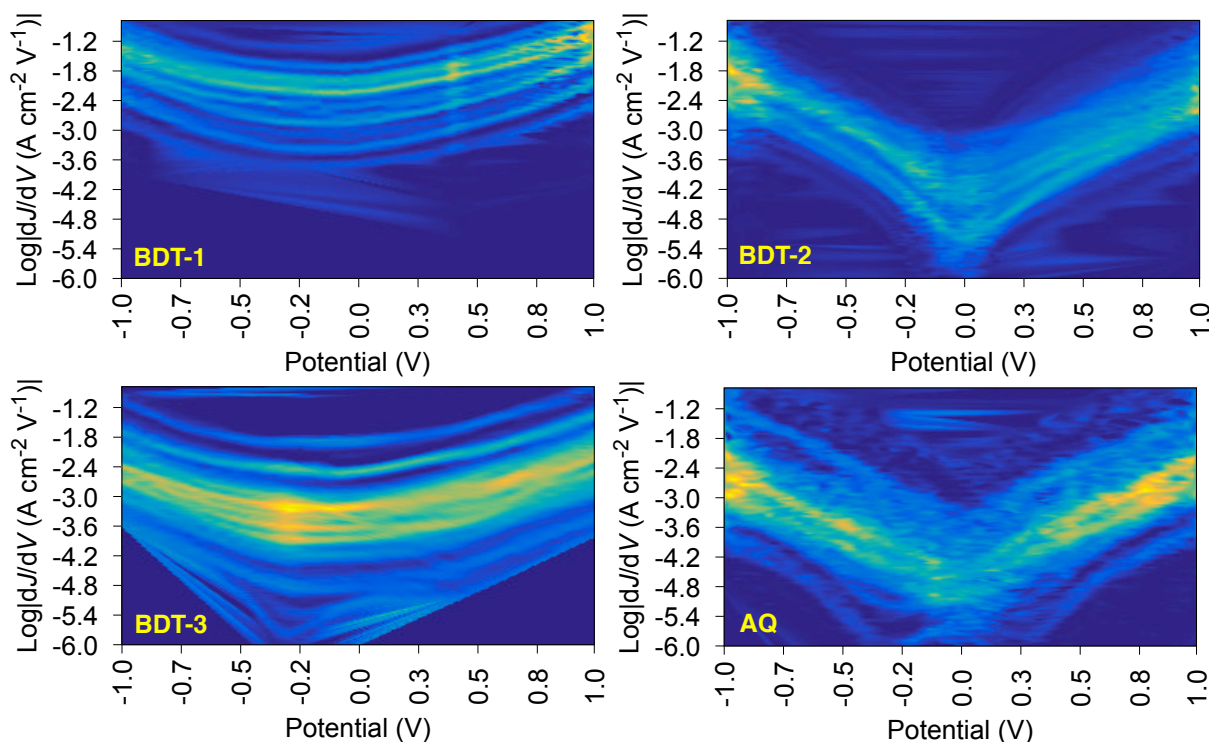


Figure 4: Differential conductance heatmap plots of Au/SAM//EGaIn junctions comprising **BDT-1** (top-left), **BDT-2** (top-right), **BDT-3** (bottom-left) and **AQ** (bottom-left) showing histograms binned to  $\log |dJ/dV|$  (differential conductance, Y-axis) versus potential (V, X-axis). The colors correspond to the frequencies of the histograms and lighter (more yellow) colors indicate higher frequencies. The bright spots near  $\pm 1$  V are due to the doubling of data that occurs in the forward/return  $J/V$  traces. The plots for both **BDT-2** and **AQ**, which contain quinones, are V-shaped at low bias and exhibit negative curvature, indicating a destructive QI feature near  $E_F$ , while the plots of **BDT-1** and **BDT-3** are U-shaped.



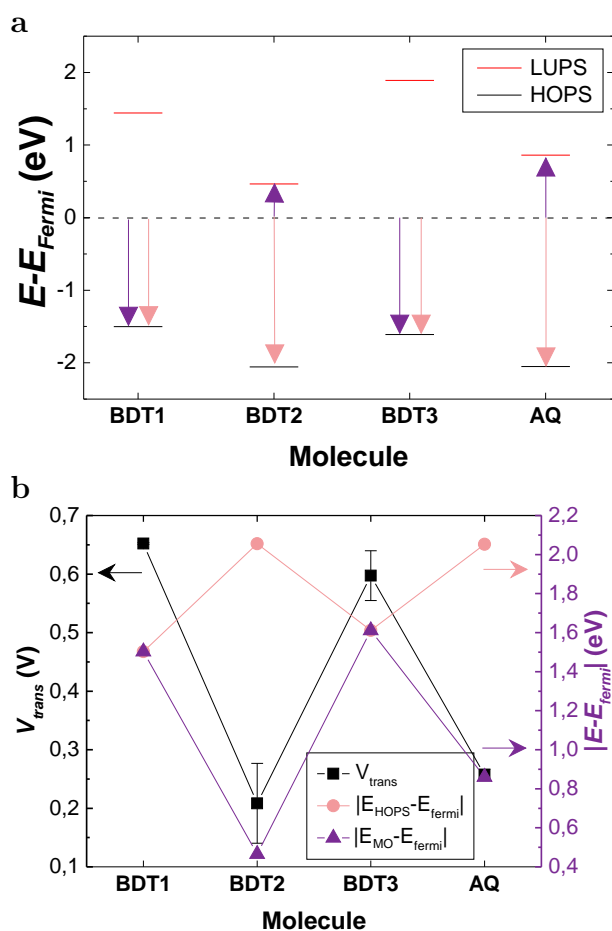


Figure 5: (a) Energy offsets of the frontier orbitals calculated using DFT with respect to  $E_{\text{F}}$  value of  $-4.3$  eV. (b) The energy offsets (salmon and purple lines, right axis) plotted with the measured values of  $V_{\text{trans}}$  (black line, left axis). The salmon line plots the energy offsets of the HOPS. The purple line plots the smallest energy difference (purple arrows in Figure 5a);  $|E_{\text{HOPS}} - E_{\text{Fermi}}|$  for **BDT-1** and **BDT-3**,  $|E_{\text{LUPS}} - E_{\text{Fermi}}|$  for **BDT-2** and **AQ**. The exact values of  $V_{\text{trans}}$  and the orbital energies are shown in Table S3 and S5.

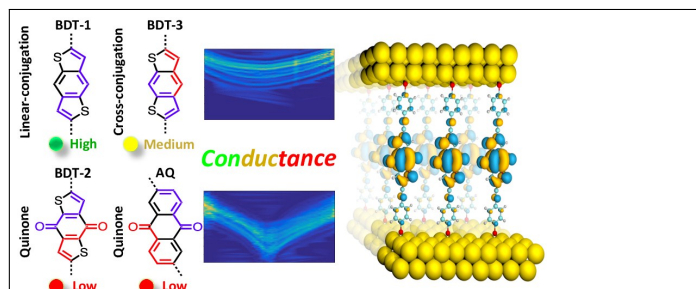


Table 1: Summary of the properties of SAMs of **BDT-*n*** and Au/**BDT-*n***/EGaIn junctions.

Compound	BDT-1	BDT-2	BDT-3	C18 reference
XPS thickness (Å)	17 ± 3	18 ± 4	19 ± 4	n.d.
HRXPS thickness (Å)	19.81 ± 0.40	22.30 ± 0.45	17.17 ± 0.34	20.9
Averaged XPS thickness (Å)	18.4	20.2	18.4	n.d.
Water contact angle (°)	68.3 ± 4.8	65.8 ± 4.0	62.8 ± 4.6	104.2 ± 2.2
Density (10 <sup>14</sup> molecules per cm <sup>2</sup> )	2.05	3.30	2.33	4.63
Area molecules per Å <sup>2</sup> )	48.8 ± 2	30.3 ± 2	43.0 ± 2	21.6
log   <i>J</i>   @0.5 V (Acm <sup>-2</sup> )	-2.34 ± 0.17	-4.09 ± 0.23	-3.53 ± 0.20	-4.96 ± 0.87 <sup>[41]</sup>
Yield of working junctions (%)	88.9	93.8	84.2	79 <sup>[41]</sup>
Num. working EGaIn junctions	32	30	32	28 <sup>[41]</sup>
Total <i>J/V</i> traces	643	626	666	280 <sup>[41]</sup>



## Graphical TOC Entry



## Table of Contents

Three different benzodithiophene derivatives were designed to isolate the effects of bond topology from that of functional groups in quantum interference to examine the role of the quinone functionality separate from cross-conjugation in SAMs based large area molecular junctions. Quinones are found to suppress tunneling transport further than cross-conjugation alone and to switch the mechanism from tunneling mediated by occupied states to tunneling mediated by unoccupied states.

